iScience

CellPress

Article

The Complement Regulator *Susd4* Influences Nervous-System Function and Neuronal Morphology in Mice

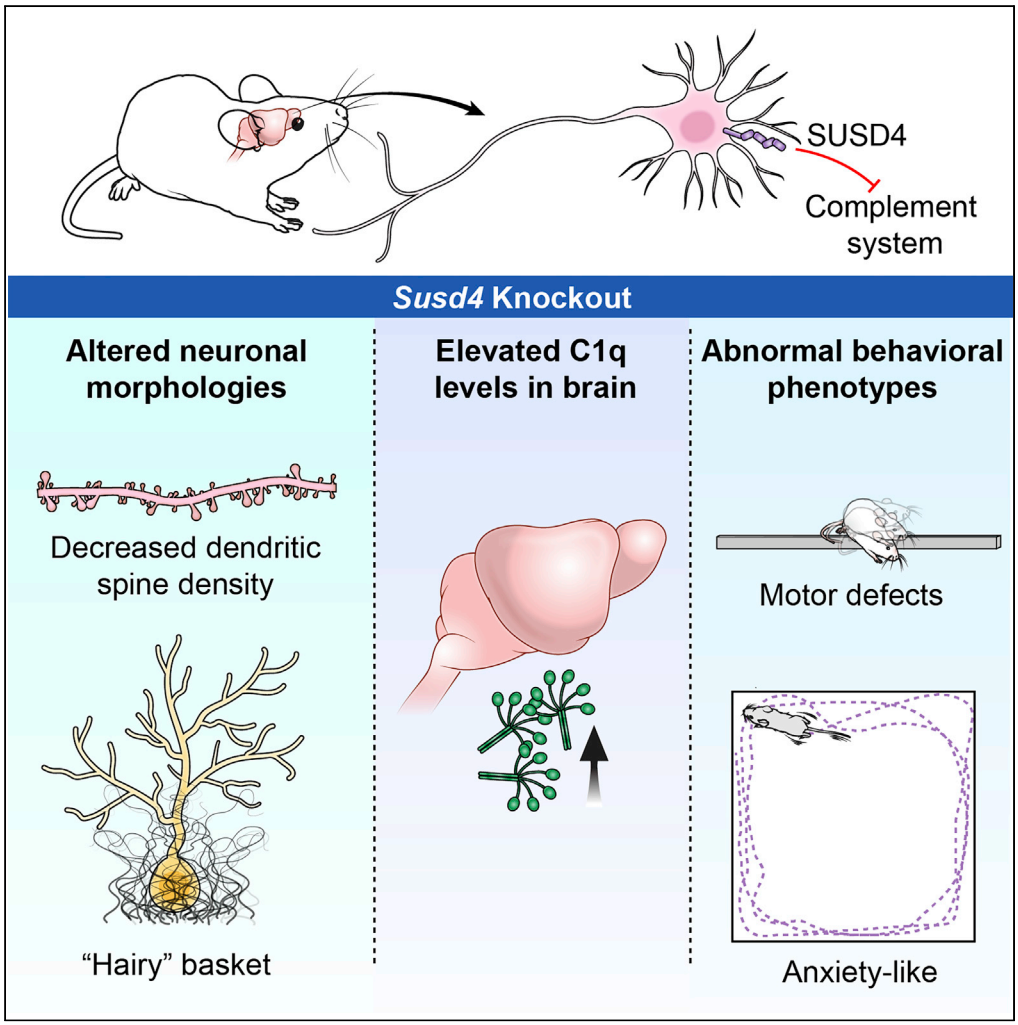

Hongling Zhu, Laura E. Meissner, Colleen Byrnes, Galina Tuymetova, Cynthia J. Tifft, Richard L. Proia

cynthiat@mail.nih.gov (C.J.T.)
proia@nih.gov (R.L.P.)

HIGHLIGHTS

Susd4 is expressed in neurons and oligodendrocyte lineage cells

Susd4 knockout mice have abnormal hippocampal and cerebellar neuronal morphologies

Susd4 knockout mice exhibit anxiety-like behaviors and impaired motor function

Susd4 knockout mice have elevated brain levels of the complement component C1q

Zhu et al., iScience *23*, 100957
March 27, 2020
https://doi.org/10.1016/j.isci.2020.100957

iScience

CellPress

Article

The Complement Regulator *Susd4* Influences Nervous-System Function and Neuronal Morphology in Mice

Hongling Zhu,[1] Laura E. Meissner,[2] Colleen Byrnes,[1] Galina Tuymetova,[1] Cynthia J. Tifft,[2,*] and Richard L. Proia[1,3,*]

SUMMARY

The *SUSD4* (Sushi domain-containing protein 4) gene encodes a complement inhibitor that is frequently deleted in 1q41q42 microdeletion syndrome, a multisystem congenital disorder that includes neurodevelopmental abnormalities. To understand SUSD4's role in the mammalian nervous system, we analyzed *Susd4* knockout (KO) mice. *Susd4* KO mice exhibited significant defects in motor performance and significantly higher levels of anxiety-like behaviors. *Susd4* KO brain had abnormal "hairy" basket cells surrounding Purkinje neurons within the cerebellum and significantly reduced dendritic spine density in hippocampal pyramidal neurons. Neurons and oligodendrocyte lineage cells of wild-type mice were found to express *Susd4* mRNA. Protein expression of the complement component C1q was increased in the brains of *Susd4* KO mice. Our data indicate that SUSD4 plays an important role in neuronal functions, possibly via the complement pathway, and that *SUSD4* deletion may contribute to the nervous system abnormalities in patients with 1q41q42 deletions.

INTRODUCTION

The complement system, a critical part of the immune system, helps defend against invading pathogens, promote inflammation, and clear damaged cells and debris (Hajishengallis et al., 2017; Holers, 2014). In the central nervous system (CNS), complement components have been found to play important roles in neuron survival and synaptic pruning under both normal and disease conditions (Hong et al., 2016; Lui et al., 2016; Schafer et al., 2012; Stevens et al., 2007). However, the regulatory mechanisms for complement expression and function in the CNS are still largely unknown.

The *SUSD4* (Sushi domain-containing protein 4) gene resides on chromosome 1q41 and encodes a 49-kD transmembrane protein containing four extracellular Sushi domain motifs (Tu et al., 2010). The Sushi domain, also known as the complement control protein domain, is commonly involved in protein-protein interactions. Many complement regulators are constructed with complement control protein domains (Gialeli et al., 2018; Kirkitadze and Barlow, 2001). SUSD4 functions as a complement system regulator, as it has been shown to bind to the C1 complex and complement component C1q and block the activation of the complement cascade by interrupting the formation of C3 convertase (Holmquist et al., 2013). However, SUSD4 has also been reported to inhibit the alternative pathway warranting further studies to clarify the SUSD4 mechanisms of action on the complement system.

In humans, the CNS is a major site of SUSD4 expression (Holmquist et al., 2013). Deletion of the *SUSD4* gene, together with several other genes, frequently occurs in patients with 1q41q42 microdeletion syndrome (Shaffer et al., 2007), who generally exhibit seizures, significant developmental delay, and intellectual disability, as well as multiple congenital abnormalities, along a variable phenotypic spectrum. It is not known if *SUSD4*, when included in the deletion interval, contributes to the patients' clinical presentation. Because the physiologic role of SUSD4 in the mammalian nervous system was not yet established, we used *Susd4* knockout (KO) mice to identify the neurologic functions of *Susd4*. We found that *Susd4* deletion affects both behavioral phenotypes and neuronal morphology in these mice, demonstrating an important CNS role for SUSD4, and that its deletion may contribute to the phenotypic spectrum of patients with 1q41q42 microdeletion syndrome.

[1]Genetics of Development and Disease Branch, National Institute of Diabetes and Digestive and Kidney Diseases, Bethesda, MD 20892, USA

[2]Office of the Clinical Director and Medical Genetics Branch, National Human Genome Research Institute, National Institutes of Health, Bethesda, MD 20892, USA

[3]Lead Contact

*Correspondence: cynthiat@mail.nih.gov (C.J.T.), proia@nih.gov (R.L.P.)

https://doi.org/10.1016/j.isci.2020.100957

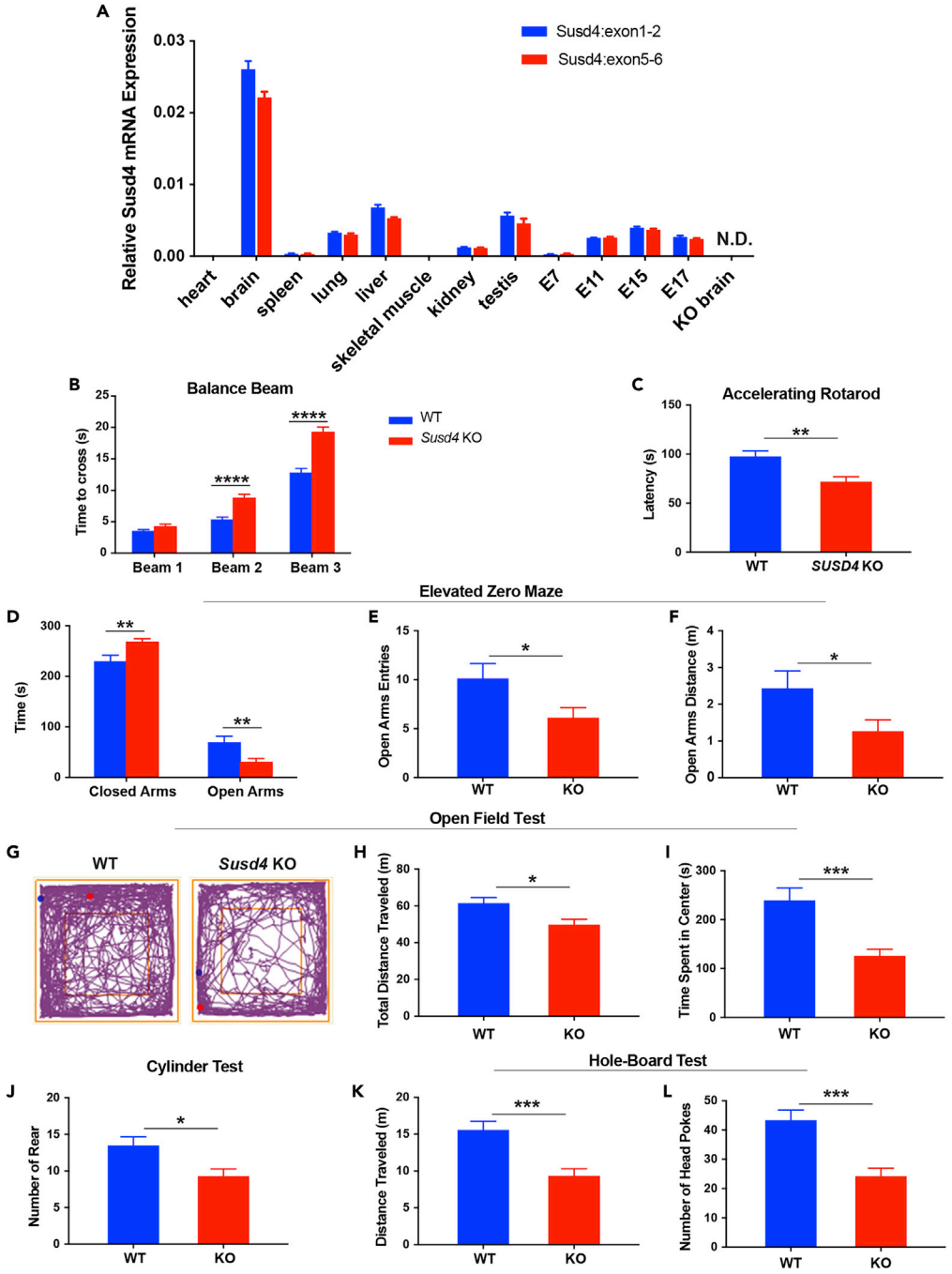

Figure 1. *Susd4* KO Mice Exhibit Behavioral Abnormalities

(A) Relative mRNA expression of Susd4 determined by qPCR in a panel of 12 different tissues from WT mice, as well as *Susd4* KO mouse brain tissue (far right). qPCR assays for Susd4 were performed using probes spanning exons 1 and 2 ($Susd4_{exon1\text{-}2}$) and exons 5 and 6 ($Susd4_{exon5\text{-}6}$) (n = 3). mRNA expression was normalized to Gapdh mRNA expression. E, embryonic day; N.D., not detectable.

(B) Horizontal balance-beam test. Time for mice to cross 80-cm-long beams of different widths was recorded. Width of the beams: beam 1 is 24 mm; beam 2 is 12 mm; beam 3 is 9.5 mm. *Susd4* KO, n = 17; WT, n = 11.

(C) Accelerating-rotarod test. Latency time for mice to fall from the rotarod was recorded. *Susd4* KO, n = 17; WT, n = 15.

(D–F) Elevated zero-maze test. (D) Time mice spent in closed and open arms of the maze was recorded for 5 min. (E) Number of open-arm entries by mice was recorded for 5 min. (F) Total distance mice traveled in the open arms was recorded for 5 min *Susd4* KO, n = 17; WT, n = 15.

Figure 1. *Continued*

(G–I) Open-field test. (G) Representative tracing of the path traveled by a WT and a *Susd4* KO mouse over 30 min in the test. The blue dot represents the starting point and the red dot represents the endpoint of the path. (H) Total distance mice traveled was recorded for 30 min. (I) Time mice spent in the center of the field was recorded for 30 min *Susd4* KO, n = 17; WT, n = 15.

(J) Cylinder test. Number of rears by mice was recorded for 90 s *Susd4* KO, n = 17; WT, n = 15.

(K and L) Hole-board test. (K) Total distance mice traveled was recorded for 5 min. (L) Number of head pokes by mice into holes was recorded for 5 min *Susd4* KO, n = 17; WT, n = 15.

Data represent the mean ± SEM. *: $p < 0.05$; **: $p < 0.005$; ***: $p < 0.0005$; ****: $p < 0.0001$. For a complete behavioral phenotyping battery, see also Table S1 and Figure S1.

RESULTS

Susd4 KO Mice Exhibit Behavioral Abnormalities

We first determined the relative tissue expression of *Susd4* mRNA in wild-type (WT) mice using qPCR (targeting exon 1–2 and exon 5–6 junctions) (Figure 1A). *Susd4* mRNA expression was highest in the WT brain and was detectable at lower levels in lung, liver, kidney, and testis, as well as during development from embryonic day 11–17.

To identify the physiologic functions of the *Susd4* gene, we utilized a *Susd4* KO mouse model (Tang et al., 2010). Expression of *Susd4* mRNA was not detectable in *Susd4* KO mouse brain, confirming the presence of a null *Susd4* allele (Figure 1A, far right). *Susd4* KO mice were viable, fertile, and grew normally (Tang et al., 2010) (see also Table S1). We subsequently performed behavioral phenotyping to determine if the *Susd4* deletion would affect nervous-system functions. Compared with WT mice, *Susd4* KO mice exhibited defects in motor and coordination function, as revealed by horizontal balance-beam and accelerating-rotarod tests. In the balance-beam test, as the width of the balance beam decreased, which increased the demand for fine locomotor control, the mean time that the *Susd4* KO mice spent to cross the beam was significantly longer than that of WT mice (Figure 1B). In the accelerating-rotarod test, the mean latency time that *Susd4* KO mice stayed on the rotarod as it accelerated was significantly shorter, indicating poorer motor coordination, than that of WT mice (Figure 1C). Gross sensorimotor and locomotor functions were not affected as assessed by Shirpa screening and DigiGait tests (Table S1, Figures S1A and S1B).

Further behavioral testing indicated that *Susd4* KO mice exhibited anxiety-like behavioral phenotypes (Crawley, 1985; Holter et al., 2015). In the elevated zero-maze test *Susd4* KO mice spent significantly more mean time in the closed arms (and significantly less mean time in the open arms) (Figure 1D), and the mean frequency of open-arm entries (Figure 1E) and the mean distance traveled in the open arms were significantly less than those observed in WT mice (Figure 1F). In the open-field test, both the mean total distance traveled (Figures 1G and 1H) and the mean time spent in the center of the field were significantly less for *Susd4* KO mice than for WT mice (Figures 1G and 1I). In addition, the *Susd4* KO mice undertook significantly reduced exploratory activity in the cylinder test (mean number of rears; Figure 1J) and the hole-board test (mean total distance traveled; Figure 1K) and mean number of head-poking into holes (Figure 1L) compared with WT mice. Learning and memory functions were generally not impaired in the *Susd4* KO mice as revealed by Morris water maze testing (Figure S1B).

Susd4 KO Mice Exhibit Abnormal Neuronal Morphology and Hypertrophic Microglia

Bielschowsky silver staining is a histochemical method to visualize nerve fibers and has been used in studies of Alzheimer's disease and other neurodegenerative disorders to identify axonal or neurofibrillary pathology (Spittaels et al., 1999; Switzer, 2000; Yamamoto and Hirano, 1986). Using this stain, we found an abnormal morphology of basket cells, termed "hairy" (Erickson-Davis et al., 2010), indicating a dense and tangled axonal plexus surrounding Purkinje cell soma, in the cerebellum of *Susd4* KO mice that was not found in the cerebellum of WT mice (Figure 2A). Changes in neurofilament heavy chain phosphorylation status is an indicator for axonal degeneration in neurological diseases and can be detected with the SMI-31 antibody (Dale and Garcia, 2012; Petzold, 2005; Stone et al., 2019; Wang et al., 2001). Immunostaining with SMI-31 revealed that the hairy basket cell dendrites enclosing the cell bodies of calbindin-positive Purkinje neurons in the *Susd4* KO mice prominently expressed phosphorylated neurofilament heavy chain (Figures 2B and 2C). Abnormal hairy basket cells are believed to be associated with Purkinje cell degeneration (Erickson-Davis et al., 2010), although no significant difference in the numbers of cerebellar Purkinje cells

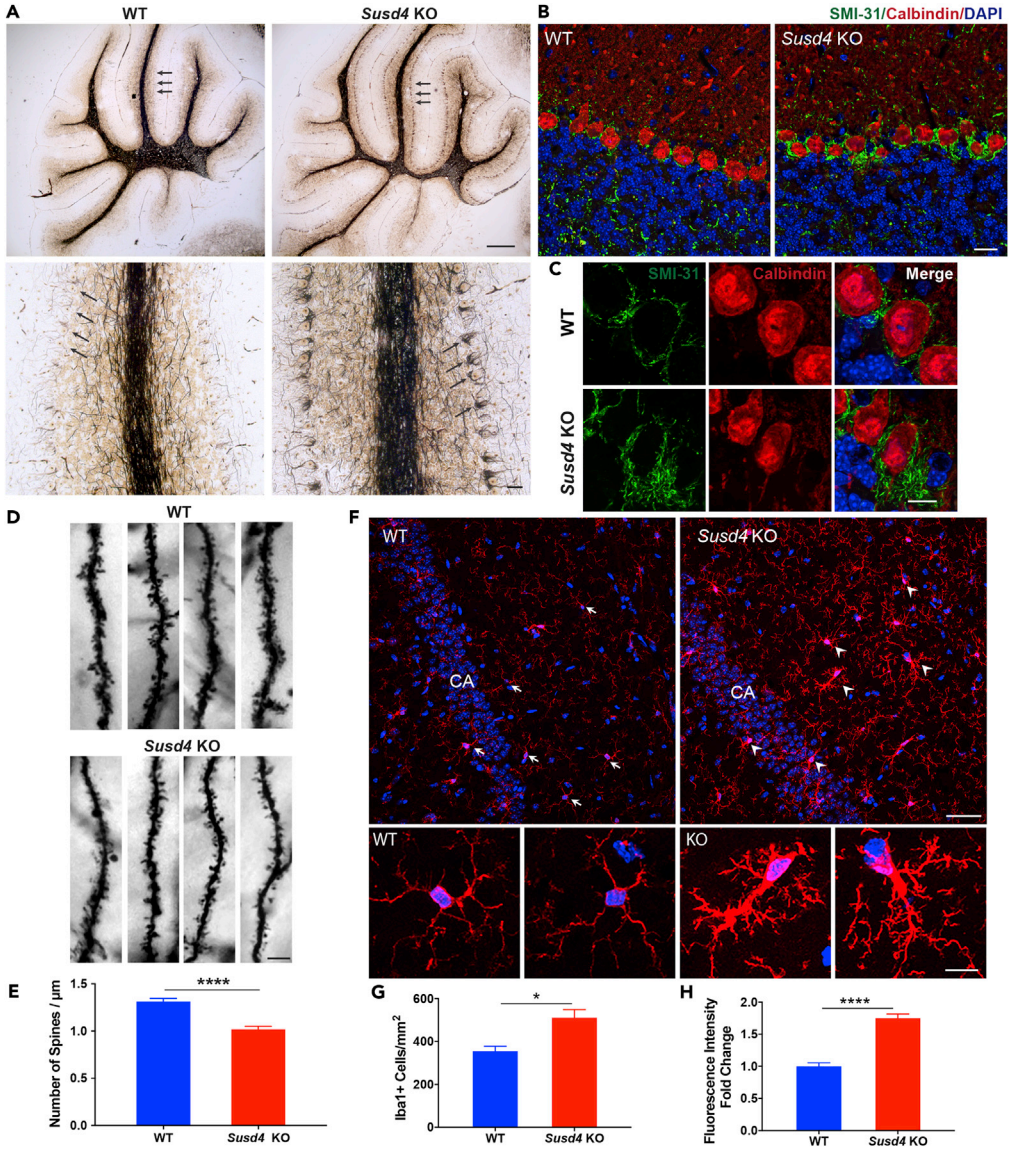

Figure 2. *Susd4* KO Mice Exhibit Abnormal Neuronal Morphology and Hypertrophic Microglia

(A) Bielschowsky silver staining of cerebellum. Top panels, representative sagittal view of the whole cerebellum for a WT and a *Susd4* KO mouse. Arrows indicate the dense-appearing basket cell layer in the *Susd4* KO mouse cerebellum relative to the WT tissue. Scale bar, 200 µm. Lower panels, representative higher magnification view shows Purkinje cell layer and basket cells (arrows). Note "hairy" appearance of basket cells in the *Susd4* KO specimen. Scale bar, 20 µm

(B) Representative immunostaining with SMI-31antibody, labeling phosphorylated neurofilament heavy chain (green), and calbindin antibody, labeling Purkinje cells (red), in cerebellum sections from *Susd4* KO and WT mice; scale bar, 20 µm.

(C) Representative higher-magnification view showing "hairy" basket cell dendrites (SMI-31 immunostaining in green) surrounding Purkinje cell soma (calbindin immunostaining in red); scale bar, 10 µm.

(D) Golgi-Cox staining of brains. Representative images of dendritic spines for WT and *Susd4* KO mice.

(E) Quantification of the number of spines per micrometer dendrite on secondary or tertiary branches from both apical and basal parts of the pyramidal cells in hippocampal CA regions of WT and *Susd4* KO Golgi-stained mouse brains. Data represent the mean ± SEM. n = 3 mice per group; ****: $p < 0.0001$.

(F) Iba1immunostaining (red) for microglia. Top panels, representative view of hippocampal regions from WT and *Susd4* KO mice. Scale bar, 40 µm. Lower panels, representative higher magnification view shows ramified resting microglia (arrows in top panel) in WT in contrast with hypertrophic microglia (arrow heads in top panel) in *Susd4* KO. CA, cornu ammonis. Scale bar, 10 µm.

Figure 2. *Continued*

(G) Quantification of Iba1+ cells per square millimeter in hippocampal regions from WT and *Susd4* KO mice. Data represent the mean ± SEM. n = 3 mice per group. *: $p < 0.05$.

(H) Quantification of Iba1 fluorescence intensity/microglia from the stained hippocampal sections. Data represent the mean ± SEM. WT values were set to 1.0. n = 3 mice per group. ****: $p < 0.0001$. Nuclei were visualized with DAPI staining (blue) for (B), (C), and (F).

in *Susd4* KO and WT mice was found (Figure S2). The abnormal basket cell morphology may be related to the motor function defects observed in *Susd4* KO mice.

The Golgi-Cox impregnation method is a classical technique used to reveal the morphology of whole individual neurons, including dendritic spines (Mancuso et al., 2013; Rosoklija et al., 2014). Dendritic spines are small protrusions that receive inputs from axons at the synapse, which are important for regulation of neuron activities and connections. Abnormalities in dendritic spines, such as changes in spine number or density, may lead to neuron degeneration and cognitive disorders (Fiala et al., 2002; Penzes et al., 2011; Skaper et al., 2017). Using the Golgi-Cox staining technique, we found a significant reduction in dendritic spine density on the pyramidal cells in hippocampal CA region in *Susd4* KO mice compared with WT mice (Figures 2D and 2E).

Microglia, resident immune cells in the brain, are involved in neuronal synaptic pruning mediated by complement factors (Tenner et al., 2018). Immunostaining of microglia with Iba1 antibodies revealed dense hypertrophic morphology of microglia in the *Susd4* KO hippocampal sections compared with the classic ramified morphology of resting microglia in the WT hippocampus (Figure 2F). The *Susd4* KO microglia were increased in number and stained more intensely with Iba1 antibody (Figures 2G and 2H). These results suggest activation of microglia in the *Susd4* KO hippocampi, a process that has been correlated with elevated synaptic pruning (Hong et al., 2016).

Susd4 Is Highly Expressed in Hippocampal Neurons and Cerebellar Purkinje Cells

Although *Susd4* is highly expressed in brain, its normal cellular expression in hippocampus and cerebellum—areas of abnormal neuronal morphology in *Susd4* KO mice—was not known. We initially tested three different commercial SUSD4 antibodies on mouse brain tissue sections, and all showed the same immunoreactivity in tissues from *Susd4* KO mice compared with WT mice, indicating a lack of sufficient antibody specificity. Therefore, we used the RNAscope Multiplex Fluorescent Assay to probe the cellular expression of *Susd4* mRNA. This *in situ* RNA hybridization assay allows simultaneous detection of three different mRNA targets per sample, with each target probe binding to a specific mRNA, each of which is then labeled with different fluorescence detectors. Initially, we used probes for Susd4 mRNA, Gfap mRNA (specific for astrocytes), and Rbfox (also known as NeuN) mRNA (specific for most neuronal types). As a specificity control for the *Susd4* probe we also hybridized sections from the *Susd4* KO mice, which showed no *Susd4* mRNA (Figure 3A). The WT mouse brain hippocampal CA layer and dentate gyrus were highly positive for NeuN mRNA (red) and *Susd4* mRNA (green) (Figure 3B). Gfap mRNA (cyan) was diffusely distributed (Figure 3B). At a higher-resolution view, *Susd4* mRNA was co-localized in cells expressing NeuN mRNA (Figure 3C) but not in cells expressing Gfap mRNA (Figure 3D). In the cerebellum of WT mice, the granular layer, which is adjacent to the Purkinje cell layer, was highly positive for NeuN mRNA (red). Purkinje cells do not express NeuN (Mullen et al., 1992). In WT mice, both the granular layer and Purkinje cell layer regions were positive for *Susd4* mRNA (green), with the large Purkinje cells showing an intense reaction. Gfap mRNA (cyan) expression was not enriched in either of these layers (Figures 3E and 3F). These results indicate that *Susd4* mRNA has relatively high expression in both hippocampal neurons and cerebellar Purkinje cells, which are areas that exhibited abnormal neuronal morphology in *Susd4* KO mice.

We next determined if *Susd4* mRNA is also expressed in the oligodendrocyte lineage using an Olig2 probe (Zhou et al., 2000). Our results indicated that a subset of Olig2-expressing cells also express *Susd4* mRNA in the cortex and corpus callosum (Figures S3A and S3B). Approximately 35% of the total Olig2+ cells in the cortex and 7.5% of the total Olig2+ in the corpus callosum were also positive for *Susd4* (Figures S3C and S3D), similar to the levels of oligodendrocyte progenitors in these regions (Young et al., 2013). Although Olig2+ cells were reduced in the *Susd4* KO cortex compared with WT, myelin basic protein (MBP) expression was found to be marginally increased in the *Susd4* KO cerebrum, suggesting the level of myelination was not adversely affected (Figures S3C and S3E). Numbers of Olig2+ cells in the corpus callosum were similar in *Susd4* KO and WT mice (Figure S3D).

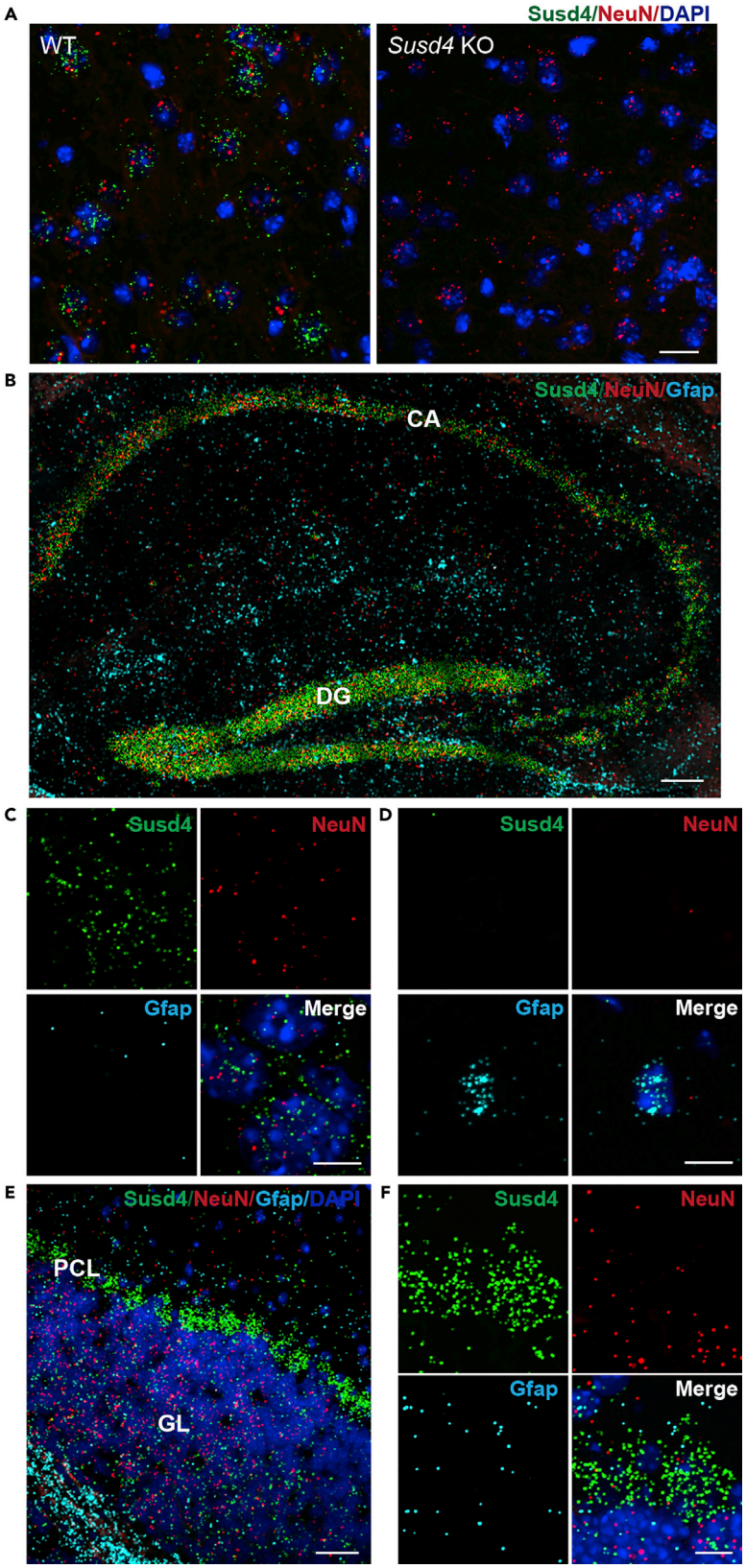
A
Susd4/NeuN/DAPI
WT
Susd4 KO
B
Susd4/NeuN/Gfap
CA
DG
C
Susd4
NeuN
Gfap
Merge
D
Susd4
NeuN
Gfap
Merge
E
Susd4/NeuN/Gfap/DAPI
PCL
GL
F
Susd4
NeuN
Gfap
Merge

Figure 3. *Susd4* mRNA is Expressed in Neuronal Cells in WT Brain

The RNAscope Multiplex Fluorescent Assay was performed with sagittal brain sections from WT and *Susd4* KO mice. Sets of probes were used to detect mRNA expression of *Susd4* (green), NeuN (red), and Gfap (cyan) *in situ*. Nuclei were visualized with DAPI staining (blue).

(A) Representative images from cortex sections show the assay specifically detects *Susd4* mRNA in WT but not in *Susd4* KO, whereas NeuN mRNA is detected in both. Scale bar, 20 μm.

(B) *Susd4* mRNA is highly expressed in the hippocampus. Scale bar, 100 μm. CA, cornu ammonis; DG, dentate gyrus.

(C and D) Representative higher-magnification views show that *Susd4* mRNA colocalizes with NeuN (C) but not Gfap (D). Scale bar, 10 μm.

(E) *Susd4*mRNA is highly expressed in Purkinje cells not the granular cells in cerebellum. Scale bar, 40 μm. PCL, Purkinje cell layer; GL, granular layer.

(F) Representative higher-magnification view shows the high expression of *Susd4* mRNA in Purkinje neurons. Scale bar, 10 μm.

Brain C1q Protein Expression Is Increased in *Susd4* KO Mice

In the nervous system, C1q is known to play critical roles in neuron dendritic pruning and synaptogenesis (Bialas and Stevens, 2013; Chu et al., 2010; Michailidou et al., 2015; Perry and O'Connor, 2008). To determine if SUSD4 expression affects C1q levels in the brain, we investigated C1q protein expression in *Susd4* KO mice by both immunostaining and western blotting. Immunostaining of hippocampal sections showed that C1q fluorescence intensity was increased 1.5-fold in the *Susd4* KO mice, when compared with WT mice (Figures 4A–4C). In the cerebellum, C1q protein was found to be relatively highly expressed in the Purkinje cells of the anterobasal lobes of the *Susd4* KO mice compared with WT (Figure 4D).

Western blotting with a monoclonal antibody to C1q indicated a 1.7-fold increase of constituent C1q expression in the cerebellum from the *Susd4* KO mice when compared with the cerebellum from WT mice (Figures 4E and 4F). C1qa mRNA levels in hippocampus and cerebellum of the *Susd4* KO mice compared with that of WT mice were not significantly different (Figures S4A and S4B), suggesting that the difference in protein levels was post-transcriptional. We investigated downstream of the complement pathway by determining complement C3 levels by western blotting of hippocampal extracts from the *Susd4* KO and WT mice. The level of C3 was not significantly different nor was there evidence of altered C3 proteolysis (Figures S4C and S4D).

We determined, through co-staining of C1q and synaptic markers on *Susd4* KO and WT hippocampal sections, if there was increased deposition of C1q on neuronal synapses, which might lead to increased synaptic pruning in the *Susd4* KO brain. Co-localization analysis of inhibitory synaptic marker vesicular GABA transporter (VGAT) (Stephan et al., 2013) and C1q revealed a 2.5-fold increase of double-positive synapses in the *Susd4* KO (Figures 4G and 4H). Western blotting demonstrated that VGAT levels were decreased by about 20% in the hippocampus from the *Susd4* KO mice when compared with the hippocampus from WT mice (Figures 4I and 4J).

Co-localization analysis of excitatory synaptic marker, vesicular glutamate transporter 1 (VGlut1) and C1q revealed a 1.6-fold increase of double-positive synapses in the *Susd4* KO hippocampal sections (Figures S4G and S4H) (Stephan et al., 2013). The total VGlut1 protein level measured by western blotting was not statistically significant between *Susd4* KO and the WT hippocampus (Figures S4I and S4J). These results show that, in the absence of SUSD4, C1q levels are elevated in the brain with increased deposition at synapses, which may lead to synaptic loss through pruning.

DISCUSSION

SUSD4 has been identified as a novel complement regulator that binds to the complement component C1q (Holmquist et al., 2013; Tu et al., 2010); however, its *in vivo* roles in the CNS are still largely unknown. Here, in the *Susd4* KO mouse model we found increased C1q levels in the brain, activation status of microglia, neuronal morphology in the hippocampus and cerebellum, and motor and anxiety-like behavioral phenotypes.

The abnormal behavioral changes indicative of increased anxiety and decreased motor function observed in the *Susd4* KO mice may be a reflection of morphologic changes in brain regions, such as the hippocampus, an area known to be involved in anxiety (Bannerman et al., 2014), and the cerebellum, the control center for motor function and coordination (Manto et al., 2012). Indeed, we found that brains from *Susd4* KO mice were characterized by abnormal "hairy" basket cells surrounding Purkinje cell soma in the cerebellum, as well as decreased dendritic spine density on the pyramidal cells in the CA region of hippocampus.

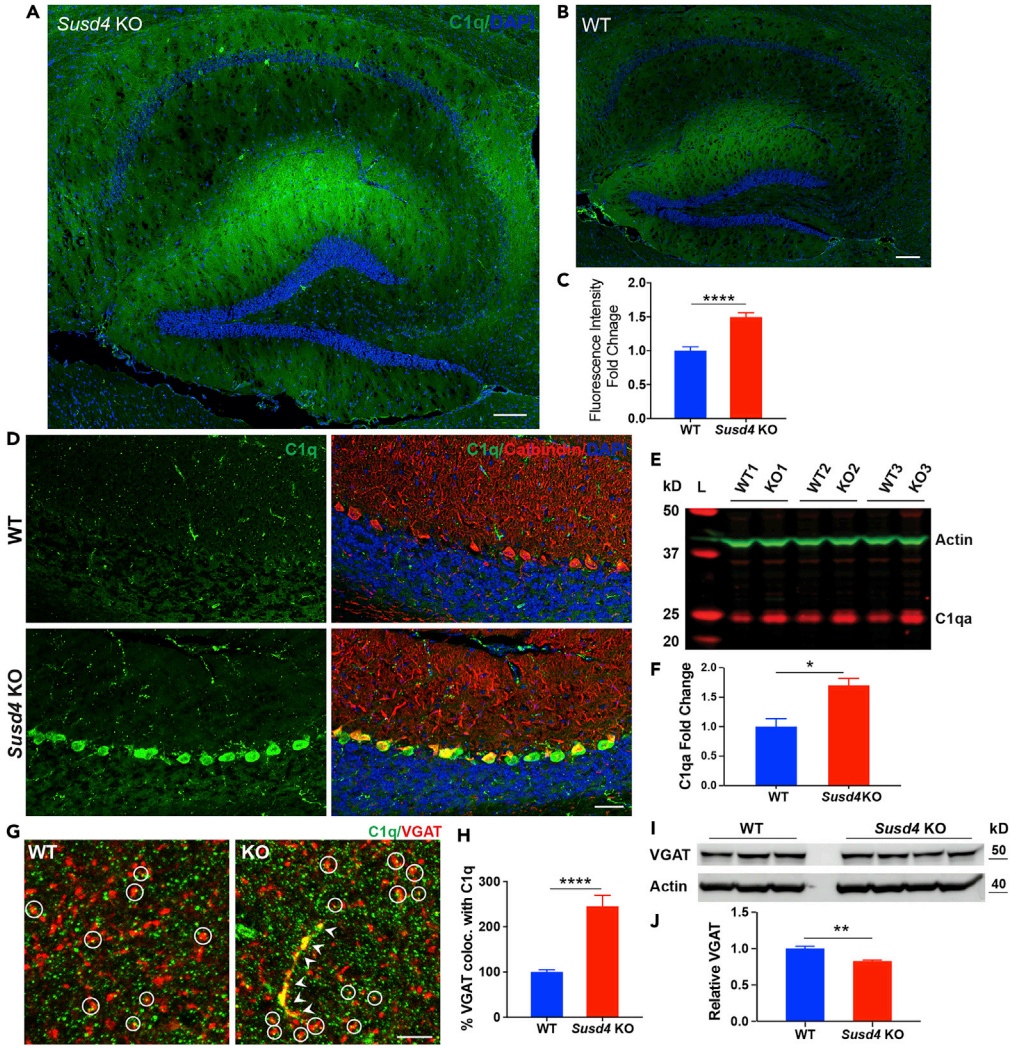

Figure 4. Brain C1q Protein Expression Is Increased in *Susd4* KO Mice

(A and B) Representative immunostaining for C1q (green) in the hippocampus sections of *Susd4* KO (A) and WT (B) mice; scale bar, 100 μm.

(C) Quantification of C1q fluorescence intensity from the stained hippocampus sections. Data represent the mean ± SEM. WT values were set to 1.0. n = 3 mice per group. ****: $p < 0.0001$.

(D) Representative immunostaining for C1q (green) and calbindin (red) in the cerebellum sections of *Susd4* KO and WT mice. Scale bar, 40 μm. Nuclei were visualized with DAPI staining (blue) for (A), (B), and (D).

(E) Western blot analysis of C1q polypeptide levels in cerebellum lysates obtained from three WT and three *Susd4* KO mice. β-Actin was simultaneously detected on the same blot as a loading control. L, molecular weight ladder.

(F) Quantification of C1q polypeptide expression from western blots. Expression was normalized to β-actin expression. Data represent the mean ± SEM. WT values were set to 1.0. *: $p < 0.05$.

(G) Representative immunostaining for C1q (green) and VGAT (red) in the WT and *Susd4* KO hippocampal sections. Circles indicate the C1q and VGAT colocalized puncta in the sections. Arrow heads point to dendrite colocalized C1q and VGAT in the *Susd4* KO section. Scale bar, 5 μm.

(H) Quantification using ImageJ of percentage VGAT colocalized with C1q. Data represent the mean ± SEM. n = 3 mice per group. ****: $p < 0.0001$.

(I) Western blot analysis of VGAT in hippocampal lysates obtained from three WT and four *Susd4* KO mice. β-Actin was detected on the same blot as a loading control.

(J) Quantification of VGAT protein levels from western blots. Expression was normalized to β-actin expression. WT values were set to 1.0. **: $p < 0.005$.

The phenomenon of "hairy" basket cells in the cerebellum has been specifically described in degenerative human brains of individuals with cerebellar essential tremor that are characterized by progressive loss of Purkinje cells and degenerative axonal abnormalities (Axelrad et al., 2008; Babij et al., 2013; Kuo et al., 2017). Basket cells are GABAergic inhibitory interneurons distributed across different regions of the brain, including the cortex, hippocampus, and cerebellum. Basket cells send inhibitory synapses to the soma of target cells to control their overall potentials. Purkinje cells are the sole output of motor coordination from the cerebellar cortex (Erickson-Davis et al., 2010). Although the mechanism of increased "hairiness" of basket cells is not clear, one possibility is that it represents an accumulation of converging and reorganizing of basket-cell processes recruited from damaged Purkinje cells (Erickson-Davis et al., 2010). Similar hairy basket formation was detected in epileptic hippocampus specimens owing to loss of affected pyramidal cells innervated by the basket cells (Arellano et al., 2004; Buckmaster and Jongen-Relo, 1999). However, in the *Susd4* KO model, no apparent loss of Purkinje cells in the cerebellum occurred, indicating that SUSD4 may influence innervative synaptic formation between Purkinje and basket cells through a different mechanism.

Dendritic spines are membranous protrusions that neurons use to form the postsynaptic component of the excitatory synapse (Nimchinsky et al., 2002; Rochefort and Konnerth, 2012; von Bohlen Und Halbach, 2009). Given that spines are the site for neurons to receive synaptic transmission, changes in spine morphology and numbers can be a fundamental indicator of physiological or pathological changes in the brain (Berry and Nedivi, 2017; Herms and Dorostkar, 2016; Moser et al., 1994; Perez-Cruz et al., 2011). The molecular mechanisms that regulate spine genesis (synaptogenesis) and removal (synaptic pruning) have been intensively studied (Kilinc, 2018; Lu and Van Vactor, 2013; Sudhof, 2018). Accumulating evidence has revealed that components of the complement system (C1q, C3, and C4) and microglia play important roles in regulation of synaptic refinement and elimination during developmental synaptogenesis in the CNS (Mastellos, 2014; Presumey et al., 2017; Schafer et al., 2012; Tenner et al., 2018). Activation of complement under pathological conditions can lead to excessive synaptic pruning by microglia and neuron degeneration, as has been reported for Alzheimer's disease and other cognitive or behavioral disorders (Depboylu et al., 2011; Lian et al., 2015; Pavlovski et al., 2012). In *Susd4* KO mouse brain, we found decreased dendritic spine density in hippocampal pyramidal neurons. SUSD4 has been shown to bind to C1q, a subunit of the first component (C1 complex) for the classic complement pathway, and inhibit formation of downstream C3 convertase (Holmquist et al., 2013). The increased C1q protein expression and neuronal synaptic deposition, hypertrophic microglia, and reduced synaptic density of neurons in *Susd4* KO mice suggest that *Susd4* may regulate complement-dependent synaptic pruning by microglia.

The exact mechanism leading to the increase of C1q in the *Susd4* KO brain has not been established. The *Susd4* deletion does not affect C1qa mRNA levels indicating that the mechanism is likely post-transcriptional. One possibility is that SUSD4 can alter the C1q levels directly by accelerating C1q degradation, as described for other complement control protein-containing regulators, such as DAF/CR1 on the C3/C5 convertase and CSMD1/factor I on C4b/C3b (Escudero-Esparza et al., 2013; Noris and Remuzzi, 2013; Seya et al., 1985).

The human *SUSD4* locus resides on chromosome 1q41 and is frequently deleted in patients with 1q41q42 microdeletion syndrome (Shaffer et al., 2007). Clinical features, which occur along a variable phenotypic spectrum, generally include severe developmental delay, seizures, as well as multiple congenital abnormalities. *DISP1* (Jun et al., 2013; Kantarci et al., 2010), *TP53PB3* (Zak et al., 2016), *WDR26* (Skraban et al., 2017; Yanagishita et al., 2019), and *FOXO28* (Cassina et al., 2015; Yanagishita et al., 2019) have each been implicated as genes responsible for some features of the deletion syndrome. Although *SUSD4* was included in the original description of the smallest region of deletion overlap among patients with 1q41q42 microdeletion syndrome (Shaffer et al., 2007), further refinement has indicated that *SUSD4* is unlikely to be responsible for major features of the disease (Jun et al., 2013). However, the demonstration here that *Susd4* has important functions in the mammalian CNS raises the possibility that it may be a contributory factor in neurologic symptom severity when it is deleted in conjunction with the major causative genes in the patients with 1q41q42 microdeletion syndrome.

In summary, we have demonstrated substantial neurologic abnormalities in mice in which the *Susd4* gene has been deleted. These findings suggest an important role for SUSD4 in the CNS and that it may act through regulation of C1q functions in the CNS. Finally, the linkage of *Susd4* expression to mammalian CNS function implicates the deletion of the *SUSD4* gene as a potential phenotypic modifier in 1q41q42 microdeletion syndrome.

Limitation of the Study

We have shown that deletion of SUSD4 increases the levels of C1q in the brain. Although previously shown as an *in vitro* complement system inhibitor, the mechanism by which SUSD4 regulates the complement system and C1q levels in brain is not known and is a subject for future research.

METHODS

All methods can be found in the accompanying Transparent Methods supplemental file.

SUPPLEMENTAL INFORMATION

Supplemental Information can be found online at https://doi.org/10.1016/j.isci.2020.100957.

ACKNOWLEDGMENTS

We thank Kate Frost and Camille Wang for assistance in the early stages of the project. This work was supported by the Intramural Research Programs of the National Institutes of Health, National Institute of Diabetes and Digestive and Kidney Diseases (R.L.P.), and the National Human Genome Research Institute (C.J.T.). The content is solely the responsibility of the authors and does not necessarily represent the official views of the National Institutes of Health.

AUTHOR CONTRIBUTIONS

Conceptualization, H.Z., C.J.T., and R.L.P; Investigation, H.Z., L.E.M., C.B., and G.T.; Writing – Original Draft, H.Z.; Writing – Review & Editing, C.J.T. and R.L.P.; Supervision, C.J.T. and R.L.P.

DECLARATION OF INTERESTS

The authors declare no competing interests.

Received: March 25, 2019
Revised: October 31, 2019
Accepted: February 25, 2020
Published: March 27, 2020

REFERENCES

Arellano, J.I., Munoz, A., Ballesteros-Yanez, I., Sola, R.G., and DeFelipe, J. (2004). Histopathology and reorganization of chandelier cells in the human epileptic sclerotic hippocampus. Brain *127*, 45–64.

Axelrad, J.E., Louis, E.D., Honig, L.S., Flores, I., Ross, G.W., Pahwa, R., Lyons, K.E., Faust, P.L., and Vonsattel, J.P. (2008). Reduced Purkinje cell number in essential tremor: a postmortem study. Arch. Neurol. *65*, 101–107.

Babij, R., Lee, M., Cortes, E., Vonsattel, J.P., Faust, P.L., and Louis, E.D. (2013). Purkinje cell axonal anatomy: quantifying morphometric changes in essential tremor versus control brains. Brain *136*, 3051–3061.

Bannerman, D.M., Sprengel, R., Sanderson, D.J., McHugh, S.B., Rawlins, J.N., Monyer, H., and Seeburg, P.H. (2014). Hippocampal synaptic plasticity, spatial memory and anxiety. Nat. Rev. Neurosci. *15*, 181–192.

Berry, K.P., and Nedivi, E. (2017). Spine dynamics: are they all the same? Neuron *96*, 43–55.

Bialas, A.R., and Stevens, B. (2013). TGF-beta signaling regulates neuronal C1q expression and developmental synaptic refinement. Nat. Neurosci. *16*, 1773–1782.

Buckmaster, P.S., and Jongen-Relo, A.L. (1999). Highly specific neuron loss preserves lateral inhibitory circuits in the dentate gyrus of kainate-induced epileptic rats. J. Neurosci. *19*, 9519–9529.

Cassina, M., Rigon, C., Casarin, A., Vicenzi, V., Salviati, L., and Clementi, M. (2015). FBXO28 is a critical gene of the 1q41q42 microdeletion syndrome. Am. J. Med. Genet. A *167*, 1418–1420.

Chu, Y., Jin, X., Parada, I., Pesic, A., Stevens, B., Barres, B., and Prince, D.A. (2010). Enhanced synaptic connectivity and epilepsy in C1q knockout mice. Proc. Natl. Acad. Sci. U S A *107*, 7975–7980.

Crawley, J.N. (1985). Exploratory behavior models of anxiety in mice. Neurosci. Biobehav. Rev. *9*, 37–44.

Dale, J.M., and Garcia, M.L. (2012). Neurofilament phosphorylation during development and disease: which came first, the phosphorylation or the accumulation? J. Amino Acids *2012*, 382107.

Depboylu, C., Schafer, M.K., Arias-Carrion, O., Oertel, W.H., Weihe, E., and Hoglinger, G.U. (2011). Possible involvement of complement factor C1q in the clearance of extracellular neuromelanin from the substantia nigra in Parkinson disease. J. Neuropathol. Exp. Neurol. *70*, 125–132.

Erickson-Davis, C.R., Faust, P.L., Vonsattel, J.P., Gupta, S., Honig, L.S., and Louis, E.D. (2010). "Hairy baskets" associated with degenerative Purkinje cell changes in essential tremor. J. Neuropathol. Exp. Neurol. *69*, 262–271.

Escudero-Esparza, A., Kalchishkova, N., Kurbasic, E., Jiang, W.G., and Blom, A.M. (2013). The novel complement inhibitor human CUB and Sushi multiple domains 1 (CSMD1) protein promotes factor I-mediated degradation of C4b and C3b and inhibits the membrane attack complex assembly. FASEB J. *27*, 5083–5093.

Fiala, J.C., Spacek, J., and Harris, K.M. (2002). Dendritic spine pathology: cause or consequence of neurological disorders? Brain Res. Brain Res. Rev. *39*, 29–54.

Gialeli, C., Gungor, B., and Blom, A.M. (2018). Novel potential inhibitors of complement system and their roles in complement regulation and beyond. Mol. Immunol. *102*, 73–83.

Hajishengallis, G., Reis, E.S., Mastellos, D.C., Ricklin, D., and Lambris, J.D. (2017). Novel mechanisms and functions of complement. Nat. Immunol. *18*, 1288–1298.

Herms, J., and Dorostkar, M.M. (2016). Dendritic spine pathology in neurodegenerative diseases. Annu. Rev. Pathol. *11*, 221–250.

Holers, V.M. (2014). Complement and its receptors: new insights into human disease. Annu. Rev. Immunol. *32*, 433–459.

Holmquist, E., Okroj, M., Nodin, B., Jirstrom, K., and Blom, A.M. (2013). Sushi domain-containing protein 4 (SUSD4) inhibits complement by disrupting the formation of the classical C3 convertase. FASEB J. *27*, 2355–2366.

Holter, S.M., Einicke, J., Sperling, B., Zimprich, A., Garrett, L., Fuchs, H., Gailus-Durner, V., Hrabe de Angelis, M., and Wurst, W. (2015). Tests for anxiety-related behavior in mice. Curr. Protoc. Mouse Biol. *5*, 291–309.

Hong, S., Beja-Glasser, V.F., Nfonoyim, B.M., Frouin, A., Li, S., Ramakrishnan, S., Merry, K.M., Shi, Q., Rosenthal, A., Barres, B.A., et al. (2016). Complement and microglia mediate early synapse loss in Alzheimer mouse models. Science *352*, 712–716.

Jun, K.R., Hur, Y.J., Lee, J.N., Kim, H.R., Shin, J.H., Oh, S.H., Lee, J.Y., and Seo, E.J. (2013). Clinical characterization of DISP1 haploinsufficiency: a case report. Eur. J. Med. Genet. *56*, 309–313.

Kantarci, S., Ackerman, K.G., Russell, M.K., Longoni, M., Sougnez, C., Noonan, K.M., Hatchwell, E., Zhang, X., Pieretti Vanmarcke, R., Anyane-Yeboa, K., et al. (2010). Characterization of the chromosome 1q41q42.12 region, and the candidate gene DISP1, in patients with CDH. Am. J. Med. Genet. A *152A*, 2493–2504.

Kilinc, D. (2018). The emerging role of mechanics in synapse formation and plasticity. Front. Cell Neurosci. *12*, 483.

Kirkitadze, M.D., and Barlow, P.N. (2001). Structure and flexibility of the multiple domain proteins that regulate complement activation. Immunol. Rev. *180*, 146–161.

Kuo, S.H., Lin, C.Y., Wang, J., Sims, P.A., Pan, M.K., Liou, J.Y., Lee, D., Tate, W.J., Kelly, G.C., Louis, E.D., et al. (2017). Climbing fiber-Purkinje cell synaptic pathology in tremor and cerebellar degenerative diseases. Acta Neuropathol. *133*, 121–138.

Lian, H., Yang, L., Cole, A., Sun, L., Chiang, A.C., Fowler, S.W., Shim, D.J., Rodriguez-Rivera, J., Taglialatela, G., Jankowsky, J.L., et al. (2015). NFkappaB-activated astroglial release of complement C3 compromises neuronal morphology and function associated with Alzheimer's disease. Neuron *85*, 101–115.

Lu, C.S., and Van Vactor, D. (2013). Genetic analysis of synaptogenesis. In Comprehensive Developmental Neuroscience: Cellular Migration and Formation of Neuronal Connections, John Rubenstein and Pasko Rakic, eds. (Academic Press), pp. 537–577.

Lui, H., Zhang, J., Makinson, S.R., Cahill, M.K., Kelley, K.W., Huang, H.Y., Shang, Y., Oldham, M.C., Martens, L.H., Gao, F., et al. (2016). Progranulin deficiency promotes circuit-specific synaptic pruning by microglia via complement activation. Cell *165*, 921–935.

Mancuso, J.J., Chen, Y., Li, X., Xue, Z., and Wong, S.T. (2013). Methods of dendritic spine detection: from Golgi to high-resolution optical imaging. Neuroscience *251*, 129–140.

Manto, M., Bower, J.M., Conforto, A.B., Delgado-Garcia, J.M., da Guarda, S.N., Gerwig, M., Habas, C., Hagura, N., Ivry, R.B., Marien, P., et al. (2012). Consensus paper: roles of the cerebellum in motor control–the diversity of ideas on cerebellar involvement in movement. Cerebellum *11*, 457–487.

Mastellos, D.C. (2014). Complement emerges as a masterful regulator of CNS homeostasis, neural synaptic plasticity and cognitive function. Exp. Neurol. *261*, 469–474.

Michailidou, I., Willems, J.G., Kooi, E.J., van Eden, C., Gold, S.M., Geurts, J.J., Baas, F., Huitinga, I., and Ramaglia, V. (2015). Complement C1q-C3 associated synaptic changes in multiple sclerosis hippocampus. Ann. Neurol. *77*, 1007–1026.

Moser, M.B., Trommald, M., and Andersen, P. (1994). An increase in dendritic spine density on hippocampal CA1 pyramidal cells following spatial learning in adult rats suggests the formation of new synapses. Proc. Natl. Acad. Sci. U S A *91*, 12673–12675.

Mullen, R.J., Buck, C.R., and Smith, A.M. (1992). NeuN, a neuronal specific nuclear protein in vertebrates. Development *116*, 201–211.

Nimchinsky, E.A., Sabatini, B.L., and Svoboda, K. (2002). Structure and function of dendritic spines. Annu. Rev. Physiol. *64*, 313–353.

Noris, M., and Remuzzi, G. (2013). Overview of complement activation and regulation. Semin. Nephrol. *33*, 479–492.

Pavlovski, D., Thundyil, J., Monk, P.N., Wetsel, R.A., Taylor, S.M., and Woodruff, T.M. (2012). Generation of complement component C5a by ischemic neurons promotes neuronal apoptosis. FASEB J. *26*, 3680–3690.

Penzes, P., Cahill, M.E., Jones, K.A., VanLeeuwen, J.E., and Woolfrey, K.M. (2011). Dendritic spine pathology in neuropsychiatric disorders. Nat. Neurosci. *14*, 285–293.

Perez-Cruz, C., Nolte, M.W., van Gaalen, M.M., Rustay, N.R., Termont, A., Tanghe, A., Kirchhoff, F., and Ebert, U. (2011). Reduced spine density in specific regions of CA1 pyramidal neurons in two transgenic mouse models of Alzheimer's disease. J. Neurosci. *31*, 3926–3934.

Perry, V.H., and O'Connor, V. (2008). C1q: the perfect complement for a synaptic feast? Nat. Rev. Neurosci. *9*, 807–811.

Petzold, A. (2005). Neurofilament phosphoforms: surrogate markers for axonal injury, degeneration and loss. J. Neurol. Sci. *233*, 183–198.

Presumey, J., Bialas, A.R., and Carroll, M.C. (2017). Complement system in neural synapse elimination in development and disease. Adv. Immunol. *135*, 53–79.

Rochefort, N.L., and Konnerth, A. (2012). Dendritic spines: from structure to in vivo function. EMBO Rep. *13*, 699–708.

Rosoklija, G.B., Petrushevski, V.M., Stankov, A., Dika, A., Jakovski, Z., Pavlovski, G., Davcheva, N., Lipkin, R., Schnieder, T., Scobie, K., et al. (2014). Reliable and durable Golgi staining of brain tissue from human autopsies and experimental animals. J. Neurosci. Methods *230*, 20–29.

Schafer, D.P., Lehrman, E.K., Kautzman, A.G., Koyama, R., Mardinly, A.R., Yamasaki, R., Ransohoff, R.M., Greenberg, M.E., Barres, B.A., and Stevens, B. (2012). Microglia sculpt postnatal neural circuits in an activity and complement-dependent manner. Neuron *74*, 691–705.

Seya, T., Holers, V.M., and Atkinson, J.P. (1985). Purification and functional analysis of the polymorphic variants of the C3b/C4b receptor (CR1) and comparison with H, C4b-binding protein (C4bp), and decay accelerating factor (DAF). J. Immunol. *135*, 2661–2667.

Shaffer, L.G., Theisen, A., Bejjani, B.A., Ballif, B.C., Aylsworth, A.S., Lim, C., McDonald, M., Ellison, J.W., Kostiner, D., Saitta, S., et al. (2007). The discovery of microdeletion syndromes in the post-genomic era: review of the methodology and characterization of a new 1q41q42 microdeletion syndrome. Genet. Med. *9*, 607–616.

Skaper, S.D., Facci, L., Zusso, M., and Giusti, P. (2017). Synaptic plasticity, dementia and Alzheimer disease. CNS Neurol. Disord. Drug Targets *16*, 220–233.

Skraban, C.M., Wells, C.F., Markose, P., Cho, M.T., Nesbitt, A.I., Au, P.Y.B., Begtrup, A., Bernat, J.A., Bird, L.M., Cao, K., et al. (2017). WDR26 haploinsufficiency causes a recognizable syndrome of intellectual disability, seizures, abnormal gait, and distinctive facial features. Am. J. Hum. Genet. *101*, 139–148.

Spittaels, K., Van den Haute, C., Van Dorpe, J., Bruynseels, K., Vandezande, K., Laenen, I., Geerts, H., Mercken, M., Sciot, R., Van Lommel, A., et al. (1999). Prominent axonopathy in the brain and spinal cord of transgenic mice overexpressing four-repeat human tau protein. Am. J. Pathol. *155*, 2153–2165.

Stephan, A.H., Madison, D.V., Mateos, J.M., Fraser, D.A., Lovelett, E.A., Coutellier, L., Kim, L., Tsai, H.H., Huang, E.J., Rowitch, D.H., et al. (2013). A dramatic increase of C1q protein in the CNS during normal aging. J. Neurosci. *33*, 13460–13474.

Stevens, B., Allen, N.J., Vazquez, L.E., Howell, G.R., Christopherson, K.S., Nouri, N., Micheva, K.D., Mehalow, A.K., Huberman, A.D., Stafford, B., et al. (2007). The classical complement cascade mediates CNS synapse elimination. Cell *131*, 1164–1178.

Stone, S., Yue, Y., Stanojlovic, M., Wu, S., Karsenty, G., and Lin, W. (2019). Neuron-specific PERK inactivation exacerbates neurodegeneration during experimental autoimmune encephalomyelitis. JCI Insight *4*, 1–17.

Sudhof, T.C. (2018). Towards an understanding of synapse formation. Neuron *100*, 276–293.

Switzer, R.C., 3rd (2000). Application of silver degeneration stains for neurotoxicity testing. Toxicol. Pathol. *28*, 70–83.

Tang, T., Li, L., Tang, J., Li, Y., Lin, W.Y., Martin, F., Grant, D., Solloway, M., Parker, L., Ye, W., et al. (2010). A mouse knockout library for secreted and transmembrane proteins. Nat. Biotechnol. *28*, 749–755.

Tenner, A.J., Stevens, B., and Woodruff, T.M. (2018). New tricks for an ancient system: physiological and pathological roles of complement in the CNS. Mol. Immunol. *102*, 3–13.

Tu, Z., Cohen, M., Bu, H., and Lin, F. (2010). Tissue distribution and functional analysis of Sushi domain-containing protein 4. Am. J. Pathol. *176*, 2378–2384.

von Bohlen Und Halbach, O. (2009). Structure and function of dendritic spines within the hippocampus. Ann. Anat. *191*, 518–531.

Wang, J., Tung, Y.C., Wang, Y., Li, X.T., Iqbal, K., and Grundke-Iqbal, I. (2001). Hyperphosphorylation and accumulation of neurofilament proteins in Alzheimer disease brain and in okadaic acid-treated SY5Y cells. FEBS Lett. *507*, 81–87.

Yamamoto, T., and Hirano, A. (1986). A comparative study of modified Bielschowsky, Bodian and thioflavin S stains on Alzheimer's neurofibrillary tangles. Neuropathol. Appl. Neurobiol. *12*, 3–9.

Yanagishita, T., Yamamoto-Shimojima, K., Nakano, S., Sasaki, T., Shigematsu, H., Imai, K., and Yamamoto, T. (2019). Phenotypic features of 1q41q42 microdeletion including WDR26 and FBXO28 are clinically recognizable: the first case from Japan. Brain Dev. *41*, 452–455.

Young, K.M., Psachoulia, K., Tripathi, R.B., Dunn, S.J., Cossell, L., Attwell, D., Tohyama, K., and Richardson, W.D. (2013). Oligodendrocyte dynamics in the healthy adult CNS: evidence for myelin remodeling. Neuron *77*, 873–885.

Zak, J., Vives, V., Szumska, D., Vernet, A., Schneider, J.E., Miller, P., Slee, E.A., Joss, S., Lacassie, Y., Chen, E., et al. (2016). ASPP2 deficiency causes features of 1q41q42 microdeletion syndrome. Cell Death Differ. *23*, 1973–1984.

Zhou, Q., Wang, S., and Anderson, D.J. (2000). Identification of a novel family of oligodendrocyte lineage-specific basic helix-loop-helix transcription factors. Neuron *25*, 331–343.

iScience, Volume *23*

Supplemental Information

The Complement Regulator *Susd4* Influences Nervous-System Function and Neuronal Morphology in Mice

Hongling Zhu, Laura E. Meissner, Colleen Byrnes, Galina Tuymetova, Cynthia J. Tifft, and Richard L. Proia

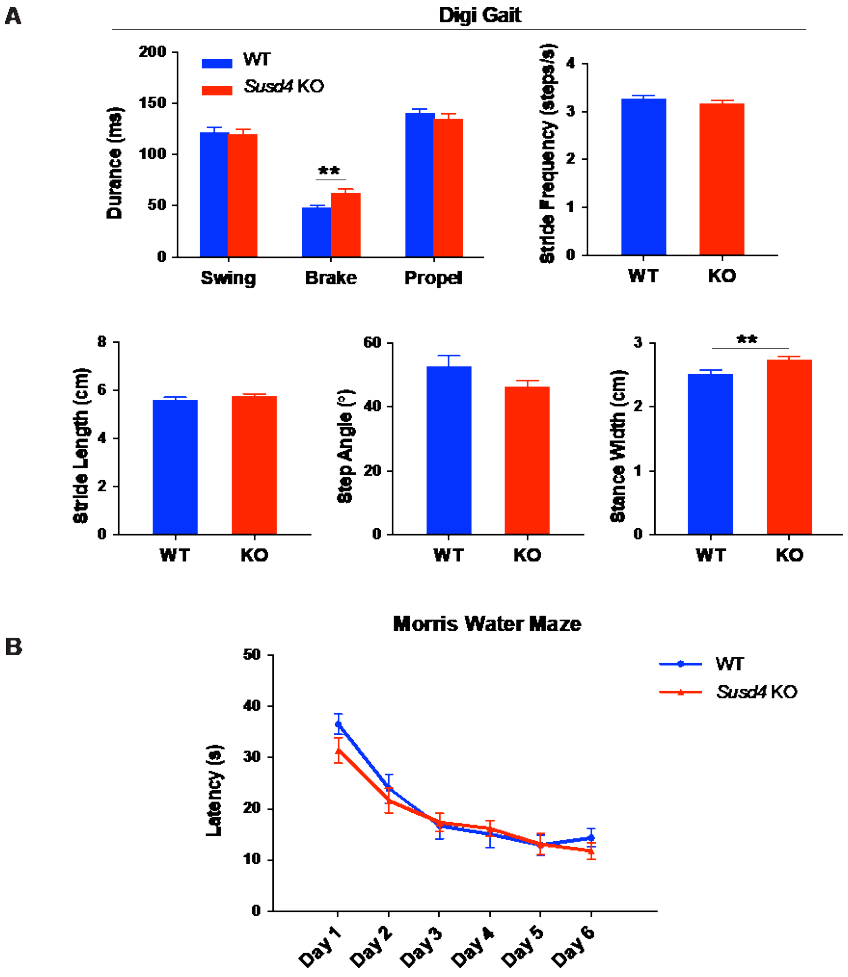

Figure S1. Behavioral phenotyping of *Susd4* KO Mice, Related to Figure 1.
(A) DigiGait test. Swing, brake, and propel of a stride, stride frequency, stride length, step angle and stance width of hind limbs were analyzed. *Susd4* KO, n=17; WT, n=11. (B) Morris water maze test. Latency to find the hidden platform was recorded for consecutive 6 training days. *Susd4* KO, n=17; WT, n=15.
Data represent the mean ± SEM. **: $p<0.005$.

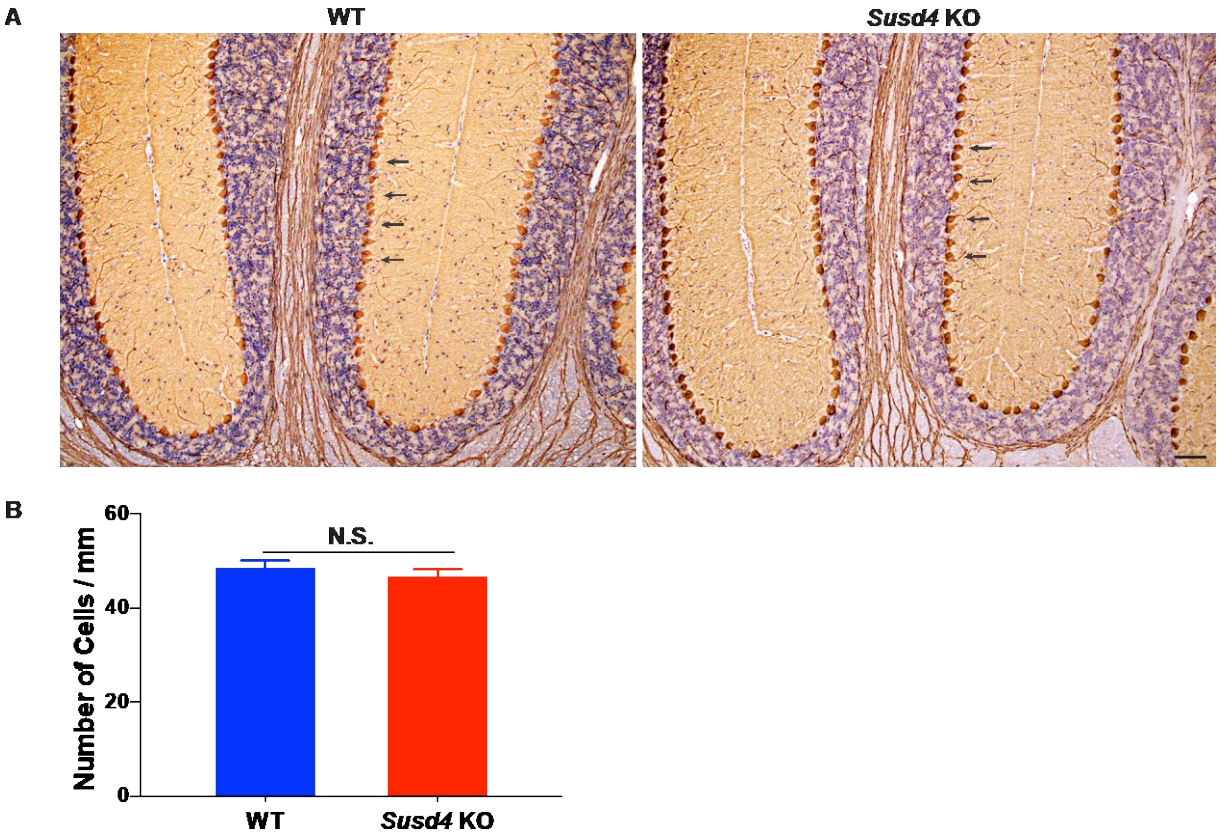

Figure S2. Purkinje Cells Are Not Lost in the Cerebellum of *Susd4* KO Mice, Related to Figure 2.
(A) Representative immunostaining for calbindin in a sagittal view of the cerebellum from a WT and a *Susd4* KO mouse. Arrows indicate calbindin-labeled Purkinje cells. Scale bar, 100 μm. (B) Quantification of the number of Purkinje cells per mm in cerebellar sections of WT and *Susd4* KO mouse brains. Data represent the mean ± SEM. n=3 mice per group. N.S.: not significant.

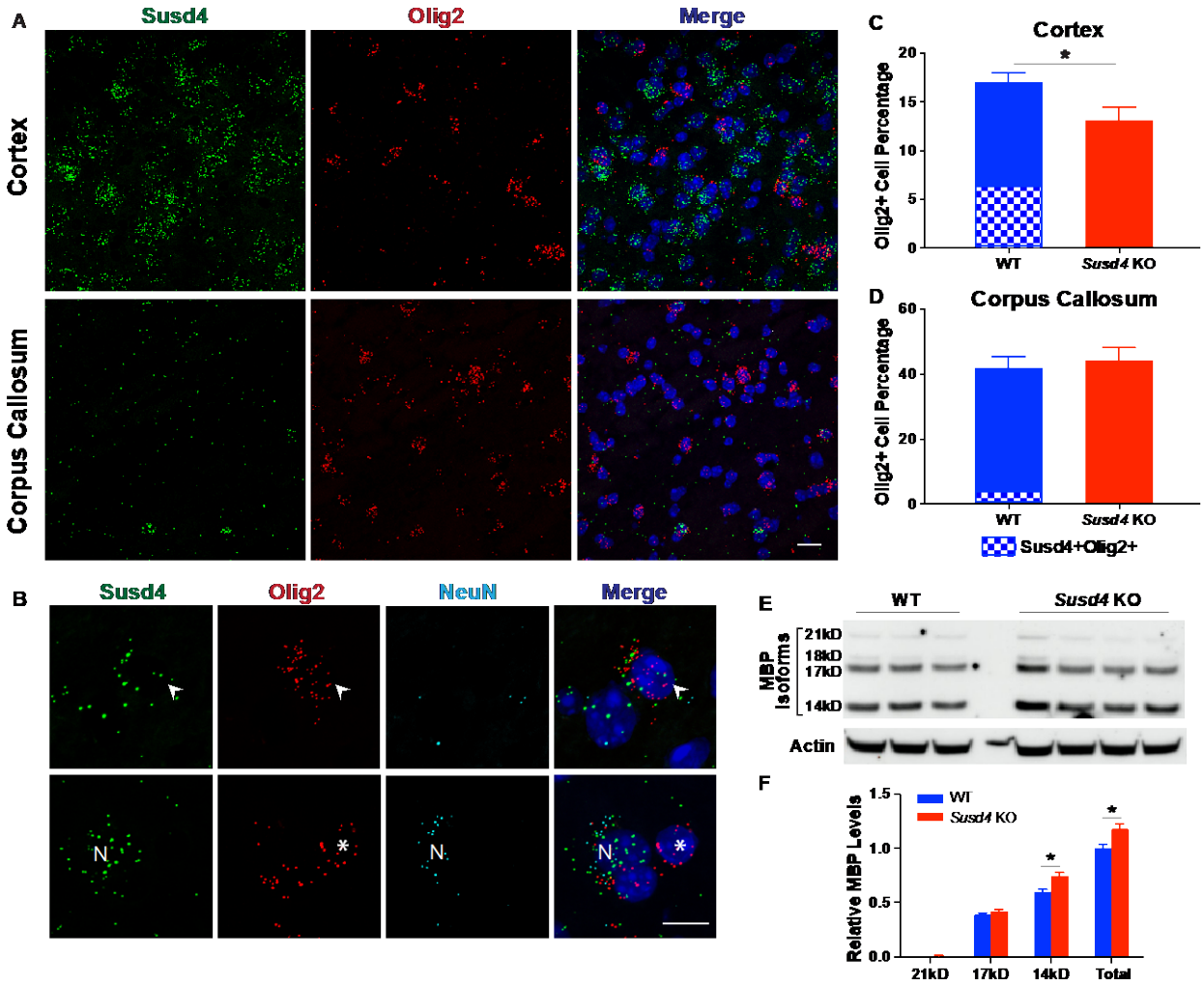

Figure S3. *Susd4* mRNA Is Expressed in Oligodendrocyte Lineage Cells, Related to Figure 3.

(A-D) Using RNAscope Multiplex Fluorescent Assay, mRNA of *Susd4* (green), Olig2 (red), and NeuN (cyan) was detected *in situ* on cerebral cortex sections from WT and *Susd4* KO mice. Nuclei were counterstained with DAPI (blue). (A) Representative images show the partially co-localized Olig2 and *Susd4* mRNA expression in WT cortex (upper panels) and corpus collosum (lower panels). Scale bar, 20 μm. (B) Representative higher magnification view shows a cell expressing both *Susd4* and Olig2 mRNA (arrow head) in upper panels, while a cell expressing Olig2 without *Susd4* (star) in lower panels. N, neuron. Scale bar, 10 μm. (C-D) Percentage of cells positive for Olig2, both positive and negative for *Susd4*, in the cerebral cortex region (C) and the corpus collosum region (D) of WT and *Susd4* KO mouse brains. Total cells were quantified by counting DAPI stained nuclei. Data represent the mean ± SEM. n=3 mice per group. (E) Western blot analysis of myelin basic protein (MBP) isoforms (21, 18, 17, and 14 kD) in cerebral cortex lysates obtained from 3 WT and 4 *Susd4* KO mice. β-actin was detected on the same blot as a loading control. (F) Quantification of MBP isoforms expression from Western blots. Expression was normalized to β-actin expression. Data represent the mean ± SEM. WT values of total MBP were set to 1.0. *: $p<0.05$

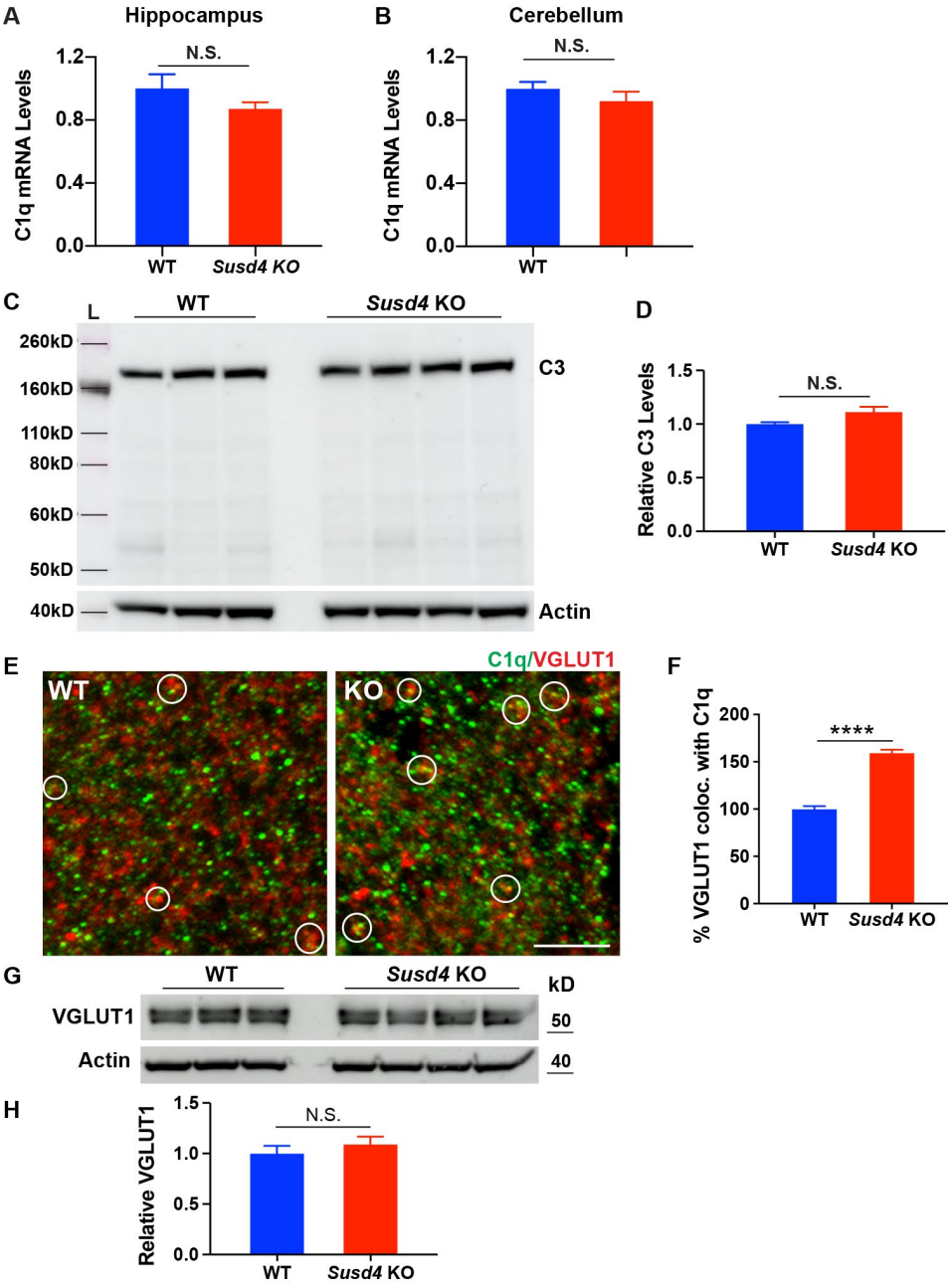

Figure S4. Determination of C1qa mRNA levels and C3 protein levels, Related to Figure 4.

(A-B) mRNA expression of C1q determined by qPCR from WT and *Susd4* KO hippocampal (A) and cerebellar (B) tissues. Expression was normalized to GAPDH expression. (C) Western blot analysis of complement C3 in hippocampal lysates obtained from 3 WT and 4 *Susd4* KO mice. β-actin was detected on the same blot as a loading control. L, molecular weight ladder sample. (D) Quantification of C3 expression (~180,000 MW band) from Western blots. Expression was normalized to β-actin expression. For A, B, and D, data represent the mean ± SEM. WT values were set to 1.0. N.S.: not significant. (E) Representative immunostaining for C1q (green) and VGLUT1 (red) in the WT and *Susd4* KO hippocampus sections. Circles indicate the C1q and VGAT colocalized puncta in the sections. Scale bar, 5 µm. (F) Quantification using ImageJ shows that % VGLUT1 found colocalized with C1q is significantly higher in *Susd4* KO. Data represent the mean ± SEM. n=3 mice per group. ****: $p<0.0001$. (G) Western-blot analysis of VGLUT1 in hippocampal lysates obtained from 3 WT and 4 *Susd4* KO mice. β-actin was detected on the same blot as a loading control. (H) Quantification of VGLUT1 protein levels from Western blots. Expression was normalized to β-actin expression. WT values were set to 1.0. N.S., not significant.

Table S1. Measures of General Health and Reflexes, Related to Figure 1.

General Health	WT (15)	*Susd4* KO (17)
Body weight (g)	26.73 ± 1.19[1]	26.41 ± 0.79
Body length: nose-tail base (cm)	9.27 ± 0.12	9.40 ± 0.04
Poor fur/skin condition (%)	0	0
Bald patches (%)	20[2]	0
Missing whiskers (%)	0	0
Piloerection (%)	0	0
Head shape (% of normal)	100	100
Nose (% of good)	100	100
Ears (% of good)	100	100
Eyes morphology (% of normal)	100	100
Teeth (% of good)	100	100
Limb (% of normal)	100	100
Tail (% of normal)	100	100
Body lumps (%)	0	0
Physical abnormality (%)	0	0
Body Temperature (°C)	35.69 ± 0.12	35.42 ± 0.07
Mucous membrane (% of normal)	100	100
Drooling (%)	0	0
Respiratory Pattern (% of normal)	100	100
Reactivity		
Eye blink (%)	100	100
Pupillary Reflex (%)	100	100
Vocalizations (%)	100	100
Biting (%)	0	0
Handling hypersensitivity (%)	0	0
Support hind end (%)	100	100
Seizures (%)	0	0
Motoric abilities		
Catalepsy test	< 1 sec	< 1 sec
Akinesia test	3.53 ± 0.69	3.80 ± 0.53
Inverted grid test[3]	90.0 ± 0.0	89.4 ± 0.6
Ladder climb test	4.52 ± 0.29	4.91 ± 0.28

1: Data represent the mean ± SEM.
2: Bald spots of 3 WT mice were caused by littermate barbering in one cage.
3: The maximum hanging time for the test is 90 sec.

TRANSPARENT METHODS

Animals

All mouse experiments were performed according to protocols approved by the Animal Care and Use Committee of the National Institute of Diabetes and Digestive and Kidney Diseases, National Institutes of Health. In the mouse facility, a 12 dark/12 light cycle was used, and mice were housed under standard conditions with *ad libitum* access to water and food.

Susd4^{tmLex} mice were obtained from Mutant Mouse Resource & Research Centers, USA (stock #: 032614-UCD, Davis, CA). The *Susd4* coding exon 1 and preceding sequence was targeted by homologous recombination to knock out the gene . For genotyping, the knockout allele was identified by PCR using 5'-GAA CAA GAT GGA TTG CAC GCA G-3' (forward primer) and 5'-CTT GAG CCT GGC GAA CAG TTC-3' (reverse primer), which generated a product of 520 bp, and the WT allele was identified using 5'-CTG TGG TTT CAA CTG GCG CTG TG-3' (forward primer) and 5'-CCG GTG GGT GTG CGA ACC TA-3' (reverse primer), which generated a product of 259 bp. The mice were backcrossed at least 7 generations into a C57BL6/J (Stock# 000664, The Jackson Laboratory, Bar Harbor, ME) genetic background for this study.

qPCR

Total RNA from mouse tissue was extracted using the RNeasy Plus Mini Kit (Qiagen, Germantown, MD). The quality and quantity of RNA was measured using the Agilent RNA 6000 Nano Kit (Agilent, Santa Clara, CA), then transcribed into cDNA with the High Capacity cDNA Reverse Transcription Kit (Applied Biosystems, Foster City, CA). TaqMan Gene Expression Assay predesigned qPCR primers and probes for mouse *Susd4* (Mm01312134_m1, Mm00460598_m1), *Gapdh* (Mm99999915_g1), and *C1qa* (Mm00432142_m1) were obtained from Applied Biosystems. qPCR was performed with a reaction volume of 20 µl and under following thermocycle conditions: 2 min of initial incubation at 50°C; 10 min initial activation and denaturation at 95°C; 40 cycles of 15 sec denaturation at 95°C, 1 min annealing and extension at 60°C. mRNA expression levels were calculated using the $\Delta\Delta C_t$ analysis method . The Susd4 tissue expression pattern was profiled using the Mouse Multiple Tissue cDNA Panel I (Takara Bio USA, Mountain View, CA), which contains a set of first-strand cDNA from 12 different tissues: heart (whole);

brain (whole); spleen; lung; liver (whole); skeletal muscle; kidney (whole); testis, 7-day embryo; 11-day embryo; 15-day embryo; and 17-day embryo.

RNAscope

The RNAscope Multiplex Fluorescent Assay (Advanced Cell Diagnostics, Newark, CA) was performed with fresh frozen 10-micron brain sections, strictly following the manufacturer's protocols. In brief, sections were first fixed in 4% paraformaldehyde for 15 min, dehydrated through serial ethanol, and permeabilized with Pretreat 4 for 30 min at room temperature. Sections were then hybridized with predesigned assay-on-demand probes of Mm-Susd4-C1, Mm-Gfap-C2 or Mm-Olig2-C2, and Mm-Rbfox3 (NeuN)-C3 (Advanced Cell Diagnostics, Newark, CA) in a HybEZ Oven (Advanced Cell Diagnostics) for 2 h at 40°C. Sections were washed twice with 1X Wash Buffer and hybridized sequentially with Amp 1-FL, Amp2-FL, Amp 3-FL, and Am 4-FL (with 2 washes in-between each hybridization). At the end, sections were counterstained with DAPI (Thermo Fisher Scientific, Rockford, IL) and mounted with ProLong Diamond Antifade Mountant (Thermo Fisher Scientific). Sections were examined and imaged on a Zeiss Axio Observer Z1 confocal microscope (Thornwood, NY). Olig2/*Susd4* labeled nuclei were counted using 'cell counter' mode of ImageJ/Fiji program (National Institutes of Health, Bethesda, MD; http://imagej.nih.gov/ij/).

Behavioral studies

All behavioral analysis was performed in the Murine Phenotyping Core Facility of the National Heart, Lung, and Blood Institute, National Institutes of Health. All tests were performed during the day light cycle on male *Susd4* KO (n=17) and WT (n=15), starting at the age of 3-5 months. Mice underwent each test one time, with a minimum of one week rest between the tests.

DigiGait analysis: Gait dynamics is a sensitive indication for locomotor deficits in diseases or drug treatments (Hampton et al., 2004). Mice were placed on a transparent treadmill positioned above a high-speed digital camera (DigiGait Imaging System, Mouse Specifics Inc., Boston MA), and run at a speed of 18 cm/sec for approximately 5 min until 12 consecutive strides were videotaped for analysis of braking, swing, and propulsion components of each stride.

Horizontal balance-beam test: This test assesses balance and coordination in mice (Luong et al., 2011). It uses a series of 80-cm-long horizontal square beams of different widths that are elevated 50 cm off the floor, with an

opaque shelter placed at the end of each beam. For acclimation, each mouse was first trained to cross a 32-mm-wide beam several times for 2 days. On the third day, each mouse was tested sequentially with beams with a width of 24 mm, 12 mm, and 9.5 mm, and the time to cross was recorded. For each mouse, the test was performed with 3 trials per beam, with a brief rest between trials and beams. One cage of 4 WT mice with barbering behavior were excluded from this test.

Accelerating-rotarod test: This test assesses motor coordination, balance, and equilibrium in mice. Each mouse was brought to the Rotamex 5 rotarod apparatus (Columbus Instruments, Columbus, OH) and first acclimated for 3 days before the test, at a steady speed of 4 rpm, 6 rpm, and up to 8 rpm (maximum 3 min/trial, 3 trials/training, with 10 min resting time between each trial). For the test, the rotarod was set at an accelerating mode (4–40 rpm, 5 min), and latency time for the mouse to fall from the rotarod was recorded. For each mouse, the test was repeated 3 times with 1 h rests between each trial.

Elevated zero-maze test: This test measures anxiety in mice (Bell et al., 2014; Kulkarni et al., 2007). The maze is a 66-cm circular runway 84 cm above the floor; part of the runway is enclosed by walls (closed arms) and other parts are open (open arms). Each mouse was placed on the runway to explore the maze for 5 min. The numbers of entries into, as well as the time and the distance the mouse traveled in, the open arms and the closed arms were recorded.

Open-field test: This test measures locomotor and anxiety-like behavior in mice (Gould et al., 2009). Each mouse was placed in a 16" × 16" × 16" Perspex chamber, and Any-maze software (version 4.99, Stoeling Co.) was used to analyze patterns of mouse movement into the center of the chamber, remaining around the edges, and the distance traveled. Each mouse was observed for 30 min and then returned to its home cage.

Cylinder test: This test assesses early sensorimotor function changes. Each mouse was placed in a small transparent cylinder (15.5-cm height; 12.7-cm diameter) and the number of spontaneous rears, which is defined as the mouse with both forelimbs off the floor and standing only on its hindlimbs, was recorded for 90 s.

Hole-board test: This test assesses anxiety and exploratory drive in mice (File and Wardill, 1975). The test uses an apparatus that is a 40 cm x 40 cm x 35 cm (height) horizontal board with multiple 3-cm holes for mice to explore. For the test, each mouse was placed in the center of the board and allowed explore the apparatus freely for 5 min. Total distance traveled and the number of head-pokings were recorded.

Morris water maze test: This test is designed for assessing spatial memory in rodents (Vorhees and Williams, 2006). It consists of a circular pool (122 cm diameter, 76 cm height) filled with room temperature water (24-30°C). Non-toxic tempura paint was added to the water to make it opaque. A 10-cm square platform was placed in northwest quadrant of the tank 1 cm beneath the water surface. Visual cues were placed around the pool for mice to locate the hidden platform. The mice were trained for consecutive 6 days with four 60-sec trials per day. Distance swam, latency to find platform, swim speed were measured by Any-maze software. On the last day, the 90-sec probe trial was performed in which the platform was removed.

Shirpa screening test battery: The modified Shirpa protocol (Rogers et al., 1997) was used as an initial non-invasive screening to observe any physical and functional abnormalities. The screening includes a gross visual inspection of fur coat, eyes, ears, teeth, nares, limbs and tail; measurement of body weight, length and temperature; a general postural assessment for body position, tremor, aggression, transfer arousal in an arena cage, grooming, freezing, rearing or jumping; sensorimotor detection of an approaching object, eye blink, ear twitch, touch escape & auditory cue; and a sequence of neuromuscular phenotyping screens including an inverted grip test to assess a mouse limb stretch by hanging it on the cage lid for a 90 sec session, a catalepsy test to place the mouse hind limbs on a raised 1.5-inch block to assess its ability to correct an abnormally imposed body position, the akinesia test to detect mobility deficit by the latency for a mouse to move all four limbs after placing it onto a flat surface, and the ladder climb test by record the time for a mouse to cross a 30 cm long metal ladder with steps placed 1.25 cm apart and positioned at a 50° angle vertically.

Histochemistry

Bielschowsky silver staining was performed by Histoserv, Inc. (Germantown, MD). For sample preparation, mice were transcardially perfused with PBS followed by 4% paraformaldehyde (PFA), then the brains were dissected and post-fixed for 48 h in 4% PFA. Brain samples were maintained in 70% ethanol and then processed into 5-micron paraffin sections for staining.

Golgi-Cox impregnation was performed with the FD Rapid Golgi Stain™ Kit by FD Neurotechnologies (Columbia, MD). Brain tissues were prepared according to the kit manual. Sagittal brain sections were cut at 100-micron thickness and examined with a Leica DMLB microscope and bright field images under a 40x objective. Neuron dendritic spine density analysis was performed with the ImageJ (Orlowski and Bjarkam, 2012). Five images of

hippocampal CA region per mouse and 3 mice per group were analyzed and spines from secondary or tertiary dendrite segments of pyramidal cells were counted using the ImageJ. Spine density was calculated using obtained spine number divided by the length of the dendrite segment.

Western blot

Dissected mouse brain cerebral, hippocampal, or cerebellar tissues were homogenized in RIPA buffer (25 mM Tris-HCl pH 7.6, 150 mM NaCl, 1% NP-40, 1% sodium deoxycholate, 0.1% SDS) with protease inhibitor cocktail (Roche, Mannheim, Germany). Lysed protein samples and molecular weight ladder (Li-Cor Biotechnology, Lincoln, NE) were heated for 10 min at 70 degrees in NuPAGE® LDS Sample Buffer containing lithium dodecyl sulfate and 50 mM dithiothreitol. Samples were separated on precast NuPAGE 4–12% Bis-Tris gels (Thermo Fisher Scientific) under denaturing conditions, and then transferred onto nitrocellulose membranes.

C1q was detected with Odyssey fluorescent western blotting (Li-Cor Biotechnology). In brief, membranes were blocked with Odyssey blocking buffer in PBS for 1 hour at room temperature, then incubated over night at 4°C with primary antibodies anti-C1q (1:50, mouse monoclonal [JL-1, cat #: MA1-40311], Thermo Fisher Scientific) and anti-β-actin (1:1000, goat polyclonal [I-19, cat #: sc-1616], Santa Cruz Biotechnology, Dallas, TX), diluted in antibody dilution buffer (Odyssey blocking buffer in PBS with 0.1% Tween 20). Membranes were washed 3 times in PBS with 0.05% Tween-20 and then incubated for 1 hour at room temperature with secondary antibodies IRDye 680LT donkey anti-mouse (1:5000, cat #: 926-68022, Li-Cor Biotechnology) and IRDye 800CW donkey anti-goat secondary antibodies (1:5000, cat #: 926-32214, Li-Cor Biotechnology). Membranes were imaged with Odyssey CLx (Li-Cor Biotechnology) and protein bands were quantified with ImageJ.

For chemiluminescent Western blotting, membranes were blocked with 5% milk for 1 hour at room temperature, then incubated over night at 4°C with primary antibodies anti-VGAT (1:10000, rabbit polyclonal [cat #: 131 002], Synaptic Systems, Goettingen, Germany), anti-VGLUT1 (1:2000, rabbit polyclonal [cat #: 12331], Cell Signaling Technology, Danvers, MA), anti-MBP(1:10000, rabbit polyclonal [cat#: PA5-78397], Thermo Fisher Scientific), anti-C3 (1:200, mouse monoclonal [cat#: sc-28294], Santa Cruz Biotechnology), Thermo Fisher Scientific), diluted in 5% milk. Membranes were washed 3 times and then incubated for 1 hour at room temperature with peroxidase conjugated secondary antibodies goat anti rabbit IgG (1:3000, cat #: AP132P, Millipore, Burlington, MA), goat anti-mouse IgG (1:2500, cat #: AP124P, Millipore), diluted in 5% milk. Membranes were detected with

ECL prime Western blotting system (Sigma-Aldrich, St. Louis, MO) and imaged with an Amersham Imager 680 (GE Healthcare Life Sciences, Pittsburgh, PA). The same membrane was then incubated for 45 min at room temperature with primary antibody anti-β-actin (1:40000, HRP conjugated mouse monoclonal [cat#: ab49900], Abcam, Cambridge, MA), diluted in 5% milk and detected with ECL.

Immunohistology

Immunofluorescent staining was done with fixed-frozen sections. Anesthetized mice were transcardially perfused with 50 ml PBS and then 100 ml 4% PFA. Brains were extracted and post-fixed in 4% PFA for 24 h at 4°C, then placed in 20% sucrose overnight or until tissues sank. Brain tissues were embedded with O.C.T. (Sakura Finetek, Torrance, CA), and 14-micron sagittal sections were cut with a cryostat (Leica, Buffalo Grove, IL) and stored at -80 °C until usage. For staining, sections were washed in PBS to remove O.C.T. and then blocked with 10% normal goat serum (Thermo Fisher Scientific) and 0.3% Triton X-100 for 1 hour at room temperature. Then sections were incubated overnight at 4°C with primary antibodies anti-C1q (1:100, mouse monoclonal [JL-1, cat #: MA1-40311], Thermo Fisher Scientific), anti-NeuN (1:1000, rabbit polyclonal [cat #: ab128886], Abcam), anti-neurofilament H, phosphorylated (1:1000, mouse monoclonal [SMI 31, cat #: 801601], BioLegend, San Diego, CA), anti-calbindin-D-28K (1:2000, rabbit polyclonal [cat #: CB-38], Swant, Marly, Switzerland), anti-Iba1(1:500, rabbit polyclonal [cat #: 019-19741], Wako, Richmond, VA), anti VGAT(1:1000, rabbit polyclonal [cat #: 131 002], Synaptic Systems) anti-VGLUT1 (1:1000, rabbit polyclonal [cat #: 135 302], Synaptic Systems), diluted in 2% normal goat serum. Sections were washed 3 times in PBS and then incubated for 1 hour at room temperature with secondary antibodies Dylight 488 goat anti-mouse (1:800, cat #:35503, Thermo Fisher Scientific), Dylight 594 goat anti-rabbit (1:800, cat #:35561, Thermo Fisher Scientific). Sections were counterstained with DAPI (Thermo Fisher Scientific) and mounted with ProLong Gold Antifade Mountant DAPI (Thermo Fisher Scientific). Sections were examined and imaged on a Zeiss Axio Observer Z1 confocal microscope (Thornwood, NY). Fluorescence intensity was quantified by ImageJ. In brief, 5-6 regions of interest per section were selected from the hippocampus of *Susd4* KO and WT mice. Measurements were made on 3-4 sections per mouse and 3 mice per group. Iba1 labeled microglia were counted using 'analyze particles' mode of image J. For the final result, 4 images per mouse and 3 mice per group were counted. Colocalization analysis of C1q and VGAT/VGLUT1 colocalization were carried out using 'colocalization threshold' mode of ImageJ.

For the analysis, high-resolution images (5-6 images per section) were taken from the same areas of hippocampi (3-4 sections per mouse) in *Susd4* KO and WT mice (3 mice per group).

For Purkinje cell quantification, sagittal sections of paraffin-embedded mouse brains were immunostained with calbindin antibody to identify Purkinje cells. Deparaffinized and rehydrated sections (5-micron) were subjected to heat-induced antigen retrieval and then stained with anti-calbindin-D-28K antibody (1:500, mouse monoclonal [cat#: CB-955], Sigma-Aldrich) overnight at 4°C. Immunohistochemical detection was performed using the Mouse on Mouse ImmPRESS™ Peroxidase Polymer Kit (cat# MP-2400, Vector Laboratories, Burlingame, CA) and counterstained with hematoxylin (cat# H-3401, Vector Laboratories) following manufacturer's instructions. Cerebellum regions were imaged with a Leica DMLB microscope (Buffalo Grove, IL) and 5 regions per mouse and 3 mice per group were analyzed using the ImageJ to determine the linear cell density (number of Purkinje cells divided by the Purkinje cell layer length).

QUANTIFICATION AND STATISTICAL ANALYSIS

Statistical analysis

All data were analyzed with Prism 7 software package (GraphPad Software, La Jolla, CA) and presented as mean ± standard error of the mean (SEM). Unpaired Student's *t* tests were performed to compare results between *Susd4* KO and WT groups. p-values < 0.05 were considered statistically significant. The number of biological replicates for each type of experiment is outlined in the figure legends.

Supplemental References

Bell, R., Duke, A.A., Gilmore, P.E., Page, D., and Begue, L. (2014). Anxiolytic-like effects observed in rats exposed to the elevated zero-maze following treatment with 5-HT2/5-HT3/5-HT4 ligands. Sci Rep *4*, 3881.

File, S.E., and Wardill, A.G. (1975). The reliability of the hole-board apparatus. Psychopharmacologia *44*, 47-51.

Gould, T.D., Dao, D.T., and Kovacsics, C.E. (2009). The Open Field Test. Neuromethods *42*, 1-20.

Hampton, T.G., Stasko, M.R., Kale, A., Amende, I., and Costa, A.C. (2004). Gait dynamics in trisomic mice: quantitative neurological traits of Down syndrome. Physiol Behav *82*, 381-389.

Kulkarni, S.K., Singh, K., and Bishnoi, M. (2007). Elevated zero maze: a paradigm to evaluate antianxiety effects of drugs. Methods Find Exp Clin Pharmacol *29*, 343-348.

Luong, T.N., Carlisle, H.J., Southwell, A., and Patterson, P.H. (2011). Assessment of Motor Balance and Coordination in Mice using the Balance Beam. Jove-J Vis Exp.

Orlowski, D., and Bjarkam, C.R. (2012). A simple reproducible and time saving method of semi-automatic dendrite spine density estimation compared to manual spine counting. J Neurosci Methods *208*, 128-133.

Rogers, D.C., Fisher, E.M., Brown, S.D., Peters, J., Hunter, A.J., and Martin, J.E. (1997). Behavioral and functional analysis of mouse phenotype: SHIRPA, a proposed protocol for comprehensive phenotype assessment. Mamm Genome *8*, 711-713.

Vorhees, C.V., and Williams, M.T. (2006). Morris water maze: procedures for assessing spatial and related forms of learning and memory. Nat Protoc *1*, 848-858.